JOURNAL OF NANO- AND ELECTRONIC PHYSICS
Vol. 7 No 1, 01014(8pp) (2015)

ЖУРНАЛ НАНО- ТА ЕЛЕКТРОННОЇ ФІЗИКИ
Том 7 № 1, 01014(8cc) (2015)

Tin Sulfide Films Obtained by Sulfurization of Electrodeposited Tin Precursors

N.P. Klochko[1,*], O.V. Momotenko[1], V.M. Lyubov[1], N.D. Volkova[2], V.R. Kopach[1], G.S. Khrypunov[1], M.V. Kirichenko[1], R.V. Zaitsev[1]

[1] *National Technical University "Kharkiv Polytechnic Institute", 21, Frunze Str., 61002 Kharkiv, Ukraine*
[2] *N. Zhukovsky National Aerospace University "Kharkiv Aviation Institute", 17, Chkalova Str., 61070 Kharkiv, Ukraine*

(Received 02 September 2014; published online 25 March 2015)

This article is devoted to the development of cost-effective and suitable for large-scale production method for obtaining thin films of tin sulfide SnS for photovoltaic applications. Thin films of SnS with the orthorhombic structure (Herzenbergite) were synthesized by sulfurization in sulfur vapor of tin films electrodeposited from a standard tinning solution. Synthesized polycrystalline SnS material was an electronic semiconductor with band gap and optical absorption coefficient optimum for utilization in solar cell.

Keywords: Tin sulfide SnS, Electrochemical deposition, Sulfurization, Precursor, Semiconductor.

PACS numbers: 68.55.Ag ,81.15.Pq

1. INTRODUCTION

Tin sulfide (SnS) is recognized by leading research groups worldwide to be a promising material of optoelectronics. Thin films of this semiconductor can be used [1-14] as the base layers of solar cells (SC) on the basis of compliance of its physical-chemical characteristics with requirements of photovoltaics up to the theoretical background of SC with the efficiency of 25 % based on SnS [8], on the one hand, and due to the cheapness and accessibility of tin and sulfur, on the other hand. SC on the basis of SnS should replace the thin-film analogues containing toxic, rare and valuable elements – SC with the base layers of cadmium telluride (CdTe) and copper, indium and gallium diselenide ($CuIn_xGa_{1-x}Se_2$).

So far, both vacuum [3-5, 13] and vapor-phase techniques [7-8] implemented by sophisticated equipment and simple and available liquid-phase chemical methods including electrochemical deposition [1, 2, 6, 9, 11, 12, 14] are used for the formation of single-phase SnS layers. At that, the majority of researchers report about the synthesis of SnS films with the orthorhombic structure (Herzenbergite, β-SnS) [3, 5, 6, 9, 11]. Nevertheless, the authors of [14] by the liquid-phase chemical deposition method have obtained SnS films with the cubic structure of zinc blende; and the group of scientists [4, 13] has produced by the hot wall vacuum method tin sulfide layers with the α-SnS orthorhombic structure. The data about the optical band gap of thin SnS films depending on the production method in accordance with different data [1-14] varies very widely – from 1.0 eV to 1.86 eV. They most often mention the optimum (for the use of this material as the SC base layer) optical band gap for direct transitions $E_g = 1.3$ eV and $E_g = 1.1$ eV – for indirect ones. The data on the conductivity type (both n-SnS and p-SnS are obtained) and electrical properties of semiconductor SnS films produced by different methods also differs greatly. Thus, in spite of the actuality of the use of thin film SnS material, it cannot be considered sufficiently studied. On the other hand, since the maximum efficiency of SC based on tin sulfide achieved for today is equal to only 2.04 % [7], one cannot talk about the existence of SnS film technology optimized for photovoltaics.

The electrochemical cathode deposition method combines simplicity, accessibility and fitness for large-scale production with well-controlled film manufacturing process. At the same time, presented in the literature numerous recipes of electrolytes for direct electrodeposition of tin sulfide SnS, for example, [1, 2, 9, 11, 12], recommend very dilute solutions with the typical concentrations of bivalent tin salt of 30 mM and sodium thiosulfate ($Na_2S_2O_3$) of 100 mM, whose composition should be strictly controlled and corrected because of the fast exhaustion during the film deposition process. The reason of the use of dilute solutions for direct SnS electrodeposition consists in the sodium thiosulfate which, as known [15-17], is decomposed in acidic medium with the release into electrolyte volume of free sulfur the more intensive, the higher its concentration is. Acidation of electrolytes is the necessary condition (pH < 7 for all recipes of SnS electrodeposition) to prevent hydrolysis of bivalent tin salts and formation of precipitates in the volume. We note that according to our experience, even dilute electrolytes for single-stage electrodeposition of tin sulfide are inclined to self-decomposition, since, as mentioned above, conditions providing $Na_2S_2O_3$ stability and those conditions which prevent hydrolysis of bivalent tin salt in solutions are mutually exclusive.

The two-stage manufacturing process of SnS layers which we have proposed consists in the electrochemical deposition of precursors in the form of tin films and further sulfurization of precursors by means of their treatment in sulfur vapor at increased temperatures. The similar approach consisting in electrodeposition or magnetron sputtering of metal layers and their further sulfurization in sulfur vapor was applied in [18, 19] for the production of photosensitive Cu_2ZnSnS_4 kesterite films used by the authors of [18, 19] as the base layers of thin film kesterite SC. Simplicity and many years' experience of use of the well-tested, including for mass production, technology of galvanic coatings are the ad-

* klochko_np@mail.ru

 © 2015 Sumy State University

vantages of the two-stage method with metal precursor electrodeposition. For example, a number of stable concentrated electrolytes [20, 21] is developed and successfully operated for electrochemical deposition of qualitative tin layers. The given work is devoted to the study of the structure, optical and electrical properties of tin sulfide films obtained by sulfurization of precursors in the form of Sn layers electrochemically deposited from a standard pyrophosphate tinning electrolyte. It is shown the possibility of simultaneous sulfurization in reactor of several plates-precursors without the use of sealed ampoules that opens the perspective of large-scale production of semiconductor tin sulfide films for the base layers of cheap and available SC.

2. EXPERIMENTAL TECHNIQUE

Stabilized DC power supply TEC 5060-1 and two-electrode electrochemical cell with stainless steel anode were used for electrodeposition of tin films. Glass substrates coated with SnO_2:F (FTO plates by TEC 7, Pilkington Inc., USA) of the size of 2 × 3 cm were served as cathodes (working electrodes). The electrochemical tinning process was performed at room temperature in the standard pyrophosphate electrolyte [20-21] containing 80 g/l of $SnCl_2$, 180 g/l of $Na_4P_2O_7$ and 50 g/l of NH_4Cl. The tin precursors' electrodeposition modes are shown in Table 1. Electrodeposited tin films of the thickness of 0.45-1.74 μm (Table 1) were light-colored and reliably bonded with the base.

The precursors sulfurization process was carried out by the vacuum universal post VUP-4M at the residual gas pressure not more than $2 \cdot 10^{-2}$ Pa. Powder S (State standard specification 1274-93) was used as the sulfur source. The working volume of the reactor placed into the vacuum chamber for sulfurization (Fig. 1) was made of quartz and supplied by the external resistance heater, cell for sulfur, three substrate holders, thermocouples for the sulfur and precursors' temperature control, and valve preventing leakage of sulfur and other possible volatile components formed during sulfurization. The weight ratios of sulfur in the reactor volume (charged into the cell) and tin in the precursors films were equal from 34 : 1 to 203 : 1 (Table 1). FTO substrates with tin layers were placed either backside to the cell with sulfur (Fig. 1a) or perpendicular to it (Fig. 1b) to prevent undesirable deposition of excess of sulfur or volatile impurities on the surface of precursors during their sulfurization. In order to reveal uniformity of the sulfurization mode in the case of three substrates simultaneously loaded into the reactor, precursor was electrodeposited on the large FTO substrate (6 × 3 cm), which then was cut into three parts and sulfurized. The samples of the series SnS 8.2: SnS 8.2.1, SnS 8.2.2 and SnS 8.2.3 were obtained in such a way. Using the resistance heater the substrate temperature was increased up to 330 °C, and heating of the cell with sulfur to the temperature of 100-110 °C occurred due to the heat transfer according to the temperature-time dependence presented in Fig. 2. The temperature of sulfur in the cell of 100 °C corresponded to the beginning of its evaporation, after that the precursor sulfurization process lasted 0.5 hour (Fig. 2). To protect the sulfurized films from oxidation, the decrease in their temperature to the room one was carried out as spontaneous cooling of the whole vacuum system. As a result of the interaction of tin and sulfur, the films thicknesses d increased after sulfurization and for different SnS layers they were equal from 0.82 to 3.18 μm (Table 1). Tin sulfide layers were dense, uniform over the surface and well bonded with the FTO substrates.

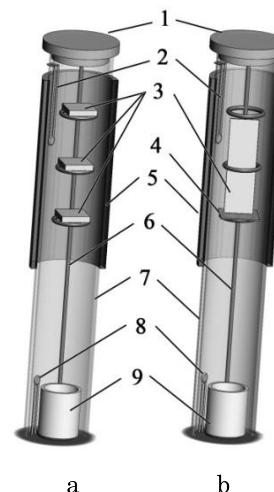

Fig. 1 – Reactors for sulfurization of tin precursors with horizontal (a) and vertical (b) arrangement of substrates: 1 – valve additionally fixed by a spring; 2 – chromel-alumel thermocouple for substrate temperature control; 3 – substrates; 4 – glass plate for substrate fixation; 5 – resistance heater; 6 – nickel-plated copper holder; 7 – quartz tube; 8 – chromel-alumel thermocouple for the temperature control of the cell with sulfur; 9 – cell with sulfur

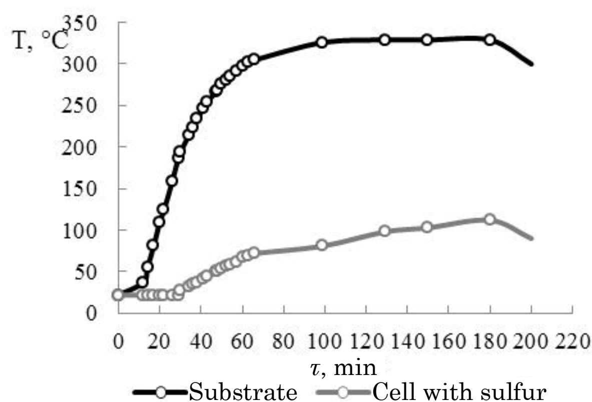

Fig. 2 – Temperature-time dependences for the cell with sulfur and tin precursors during their sulfurization

Investigation of the optical properties of sulfurized precursors was carried out using the spectrophotometer SF-2000 equipped with the add-on of specular and diffuse reflection SFO-2000. The FTO substrates were used as the test samples during the registration of the optical transmission spectra $T(\lambda)$ in the wavelength λ range from 350 nm to 1100 nm. Measurements of the reflection spectra were performed at normal light incidence. The specular and diffusion reflection spectra were summarized, and the general reflection spectra $R(\lambda)$ were obtained. Absorption coefficient α for each wavelength λ was calculated according to [14] by the following formula: $T(\lambda) = (1 - R(\lambda))^2 e^{-\alpha d}$.

Table 1 – Modes of electrochemical deposition of tin films and their sulfurization for obtaining SnS layers

Sample	Tin film electrodeposition mode			Sulfurization mode of tin films for obtaining SnS layers				
	Current density, mA/cm^2	Deposition time, s	Sn film thickness, μm	Temperature, °C	Substrates disposition	Time, hour	Mass ratio of sulfur in the cell and tin in the film, m(S)/m(Sn)	SnS film thickness d, μm
SnS 8.1	8.7	225	1.32	330	horizontal	0.5	34	2.41
SnS 8.2.1 SnS 8.2.2 SnS 8.2.3	8.9	75	0.45				167	0.82
SnS 8.3	9.8	180	1.19		vertical		103	2.17
SnS 8.4	11.5	225	1.74				107	3.18
SnS 8.5	12.0	120	0.97				203	1.77

The optical band gap E_g of SnS films was determined graphically as it is described in [2, 12] based on the relations for direct and indirect transitions:

$$(\alpha h\nu)^n = A(h\nu - E_g), \quad (1)$$

where A is the constant depending on the charge carrier effective mass in the material; $h\nu$ is the light quantum energy, eV; $n = 2$ for direct allowed optical transitions; $n = ½$ for indirect allowed optical transitions.

In order to analyze the structural and substructural parameters of precursors and sulfurized layers, the X-ray diffraction (XRD) spectra were registered by the diffractometer DRON-4M in CoKα (λCoK_α = 1.7889 Å) radiation. Scanning was carried out using the Bragg-Brentano focusing (θ-2θ). Processing of the obtained XRD patterns (background separation, splitting of Kα1 – Kα2 doublet, etc.) as well as the calculation of the parameters of the diffraction line profile were carried out using the programs "New_Profile v.3.4 (486)" and "OriginPro v.7.5". The presence of crystalline phases was revealed by the comparison of the data of the experimental XRD patterns with the master data base JCPDS using the program "PCPDFWIN v.1.30". Estimation of the coherent-scattering regions (CSR) and values of the microstresses ε in the layers was performed by the analysis of the XRD peak broadening taking into account the presence of the instrumental broadening by the Williamson-Hall approximation method according to [22-23]. Parameters of the crystal lattice were calculated by the position of two last indexed lines of the XRD patterns using the Nelson-Reilly graphical extrapolation method (NRM) and specified by the least-squares method (LSM) by the program "UnitCell" using all registered reflections of the XRD patterns according to [22-23]. Relative changes of the lattice parameters ($\Delta a/a$, $\Delta b/b$ and $\Delta c/c$) were calculated as the ratio of the difference between the experimental and reference values of the parameters of crystal lattices to their reference values.

To investigate the texture of the electrodeposited Sn precursors and SnS layers obtained by sulfurization by the Harris method, we have used the values of the integral intensities of the XRD peaks according to [22]. For each peak we have calculated the value of the pole density $P(hkl)$ characterizing the possibility with which the normal to the crystallite surface coincides with the normal to the (hkl) plane, i.e. determines the number of crystallites with the (hkl) planes parallel to the sample surface. The pole densities were determined for all registered XRD peaks; the values of $P(hkl) >> 1$ were ascribed to the texture axis.

The investigation of the surface morphology of tin precursors and tin sulfide layers obtained by sulfurization were performed using the metallurgical microscope Sigeta MM-700 which represents an inverted type of the optical microscope.

To determine the electrical properties of the manufactured tin sulfide layers we have produced ohmic contacts, the layout of which is shown in Fig.3. Rectangular indium strips with planar sizes of 2 × 6 mm were deposited by the vacuum deposition method on the SnS and FTO surface, since, according to [24], by the sum of characteristics exactly In is the most suitable contact material for SC based on SnS. Measurement of the dark dynamical current-voltage characteristics (CVC) $I = I(U)$ was carried out by the scheme of curve tracer [25]: contact device was connected with industrial curve tracer L2-56 for direct visualization of dynamical CVC of the studied sample on the screen of the electron-beam tube of this device. The general resistance $R_t = U/I$ between the contacts f and g obtained by the CVC data allowed to calculate to FTO resistivity:

$$\rho_{\text{FTO}} = R_t S/l, \quad (2)$$

where S is the area of the rectangular indium contact (S = 2 × 6 mm); l is the distance between the f and g contacts.

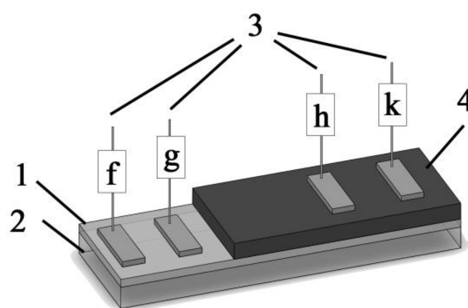

Fig. 3 – Schematic representation of the device for determination of the electrical parameters of tin sulfide layers: 1 – FTO film; 2 – glass; 3 – f, g, h, k electrodes soldered to the indium contacts; 4 – SnS semiconductor layer

Since the value of $\rho_{\text{FTO}} = 3.5 \cdot 10^{-4}$ Ohm·cm calculated based on the CVC data corresponded to the FTO rating (TEC 7, Pilkington, USA), it was taken into account in the calculations of the resistivity of tin sulfide layer ρ_{SnS}

on the basis of the CVC registered between the contacts f and h, f and k, g and h, g and k, h and k. Taking into account that based on the results of the current-voltage measurements the value of ρ_{FTO} is about seven orders less than ρ_{SnS}, in the calculations of ρ_{SnS} from the CVC registered between the contacts f and h, f and k, g and h, g and k it was assumed that from one indium contact to another current passes the distance l along the substrate over the FTO layer and overcomes the thickness d of the SnS layer (0.82-3.18 μm). Between the contacts h and k current passes twice through the SnS layer of the thickness d and overcomes the distance l over the transparent electroconductive FTO layer. In all calculations of ρ_{SnS} the value of $S = 2 \times 6$ mm was used.

Conductivity type of the SnS semiconductor material was determined by the thermoprobe method according to the standard technique [26-27]. Molybdenum rod of the length of 20 cm and diameter of 4 mm with the working end in the form of a hemisphere with a polished mirror surface of the radius of 2 mm was used as the hot probe. To provide the necessary probe temperature (60 °C), the resistive electrical heater, mounted on the part of the rod remote from the working end, was applied. Cool probe differed from the hot one by less length; its end was at the distance of ≈ 1 cm far from the point of contact of semiconductor and hot probe. Digital multimeter MASTECH MS8268 was used for the registration of the thermoelectromotive force sign. In the determination of the conductivity type of the semiconductor film, they proceeded from the known law [26] that a positive space charge appears for the electron semiconductor in the high-temperature range, since electrons diffuse from the hot region to the cool one.

3. EXPERIMENTAL RESULTS

In Fig. 4a we show two micrographs of different magnifications of the surface of precursor made of electrodeposited tin layer. The XRD analysis (Fig. 5a, Table 2) has demonstrated that tin has the tetragonal modification (JCPDS PDF#040673) typical for the films of this metal electrodeposited from pyrophosphate electrolyte [28], is a fine-grained polycrystalline material with an insignificant axial texture along the direction <100> ($P_{100} = 2.7$), microstresses ε and relative changes in the lattice parameters in which have the order of magnitudes of 10^{-3}. Electrodeposited tin films were dense, had good adhesion to the FTO substrates and covered them uniformly.

Sulfurization of tin precursors in the modes presented in Table 1 provided the formation of the well bonded with FTO dark-grey layers with smooth surface (Fig. 4b) which, according to the XRD data (Fig. 5b and Table 3), composed of polycrystalline tin monosulfide with the orthorhombic β-SnS Herzenbergite structure (JCPDS PDF#390354). Tin sulfide films were untextured and did not contain impurity phases. Calculation of the lattice parameters has revealed slightly increased values of the lattice constants and, correspondingly, the volume of the whole crystal β-SnS lattice (Table 3). Tin sulfide layer SnS 8.1 was formed twice as large crystallites (CSR = 110 nm) than the initial tin precursor. We should note that sulfurization of the SnS 8.1 sample, as well as the simultaneous sulfurization of three samples SnS 8.2.1,

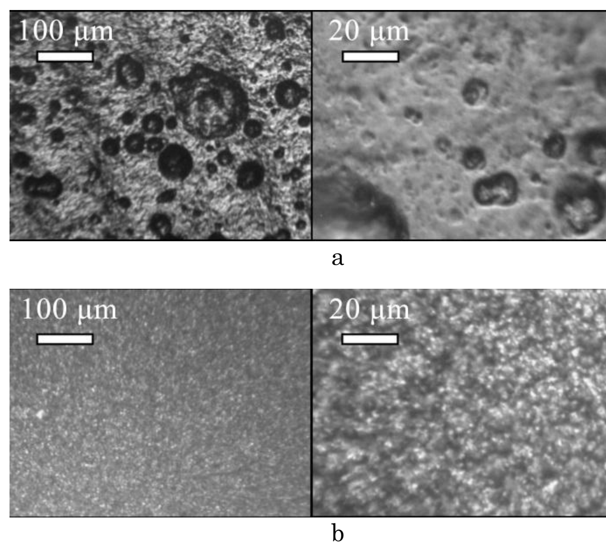

Fig. 4 – Micrographs of the surface of electrodeposited Sn precursor (d = 1.3 μm) (a) and SnS 8.1 layer (d = 2.4 μm) produced by sulfurization of this precursor (b)

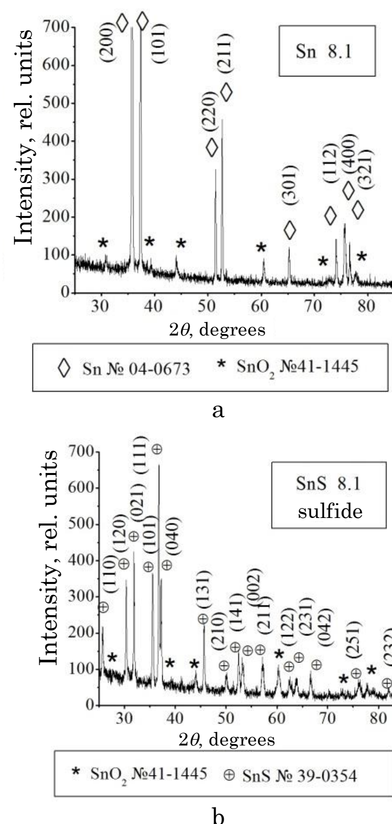

Fig. 5 – The XRD patterns of electrodeposited Sn precursor (d = 1.3 μm) (a) and SnS 8.1 layer (d = 2.4 μm) (b) obtained therefrom by sulfurization at the horizontal substrate location

SnS 8.2.2 and SnS 8.2.3, was carried out in the reactor with horizontal arrangement of the substrates backside to the cell with sulfur (Fig. 1a). In Fig. 6 we show the XRD patterns of the simultaneously sulfurized samples SnS 8.2.1, SnS 8.2.2 and SnS 8.2.3. These layers were produced of thinner tin precursors in comparison with SnS 8.1, and, therefore, they themselves were thinner that was manifested in the intensity and width of the β-SnS diffraction peaks. Grains in tin sulfide layers of

Table 2 – Typical structural characteristics of electrodeposited tin film compared with Sn standard of the tetragonal modification (JCPDS PDF#040673)

Sample	Calculation method	Lattice parameters			CSR, nm	Relative changes of the lattice parameters, 10^{-3}		ε, 10^{-3}
		a, Å	c, Å	Lattice volume, Å^3		$\Delta a/a$	$\Delta c/c$	
Sn standard JCPDS PDF#040673	–	5.831	3.182	108.19	–	–	–	–
Precursor SnS 8.1	LDM	5.82	3.16	106.99	55	2.5	6.2	1.4
	LSM	5.83	3.19	108.60		0.7	2.3	

Table 3 – Structural characteristics of tin sulfide layers compared with SnS standard of the orthorhombic modification (JCPDS PDF#390354)

Sample	Calculation method	Lattice parameters				CSR, nm	Relative changes of the lattice parameters, 10^{-3}			ε, 10^{-3}
		a, Å	b, Å	c, Å	Lattice volume, Å^3		$\Delta a/a$	$\Delta b/b$	$\Delta c/c$	
SnS standard (β-SnS JCPDS PDF#390354)		4.329	11.19	3.983	192.943	–	–	–	–	–
SnS 8.1	LDM	4.31	11.26	3.995	193.9	110	4.4	6.3	3.0	1.3-2.0
	LSM	4.31	11.23	3.995	193.5		3.7	3.3	3.0	
SnS 8.2.1	LDM	4.34	11.30	3.92	192.23	34-54	2.5	10.1	16.2	1.0-1.5
	LSM	4.32	11.26	3.97	193.61		1.0	6.2	2.3	
SnS 8.2.2	LDM	4.29	11.24	3.99	192.51	21-51	8.4	4.2	2.1	0.5-1.0
	LSM	4.32	11.21	4.00	193.59		3.0	1.9	4.5	
SnS 8.2.3	LDM	4.31	11.27	3.99	193.87	20-41	4.4	7.1	2.1	0.5-1.2
	LSM	4.31	11.22	4.00	193.18		5.5	2.2	4.6	
SnS 8.4	LDM	4.32	11.10	3.98	193.64	30-50	2.6	8	0.8	0.8
	LSM	4.31	11.24	3.99	193.64		4.2	4.8	3.0	
SnS 8.5	LDM	–	–	–	–	20	–	–	–	0.8
	LSM	4.3	11.25	4.00	193.83		6.3	5.5	5.3	–

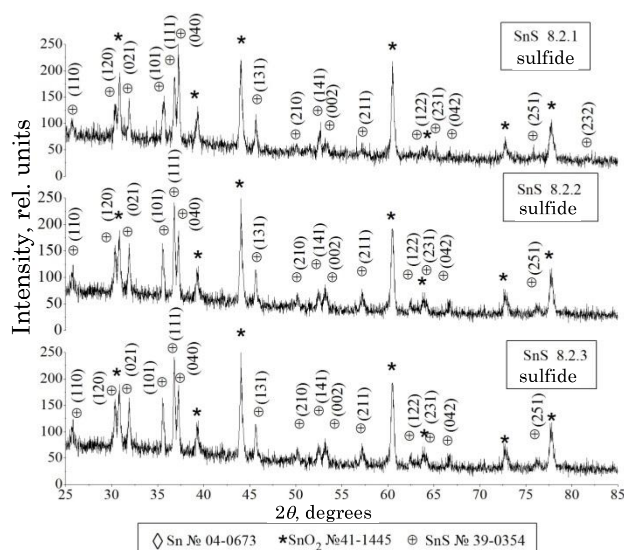

Fig. 6 – The XRD patterns of tin sulfide layers (d = 0.82 μm) obtained from electrodeposited Sn precursor (d = 0.45 μm) by simultaneous sulfurization at the horizontal arrangement of substrates

the series SnS 8.2 were smaller compared with SnS 8.1 (their CSR were equal to 20-54 nm), but microstresses ε and relative changes of the lattice parameters had the same order of magnitudes (see Table 3). None impurity phases in the SnS 8.2.1, SnS 8.2.2 and SnS 8.2.3 films were revealed. As Fig. 6 and Table 3 indicate, the structural parameters of tin sulfide layers manufactured of the same precursor and simultaneously sulfurized differed little from each other.

In the case, when sulfurization was performed at the horizontal arrangement of substrates (Fig. 1b) so that sulfur vapor rising from the cell passed along the precursors surface (SnS 8.3, SnS 8.4 and SnS 8.5 samples), we could not avoid the appearance in polycrystalline layers with the β-SnS structure of some amount of tin disulfide SnS_2 impurity of the hexagonal modification (JCPDS PDF#401467) [29-30] (Fig. 7). CSR of the β-SnS in the samples with vertical orientation of substrates were less in the sulfurization process. It is especially well seen if compare tin sulfide samples with comparable thicknesses, taking into account natural enlargement of crystallites with the increase in the precursor film thickness and, correspondingly, tin sulfide (Table 3). For a relatively thinner of sulfurized with vertical arrangement of substrates SnS 8.5 sample the halo, which indicates the presence of the X-ray amorphous phase in it, is registered on the XRD pattern (Fig. 7). A small amount of peaks on the XRD pattern of this film did not allow to perform calculations of the structural parameters by the least distance method (LDM). However, from the point of view of the texture, microstresses and distortions of the β-SnS crystal lattice, the tin sulfide layers manufactured at vertical arrangement of substrates in the sulfurization process differed little from those which were sulfurized in the reactor with horizontal arrangement of substrates.

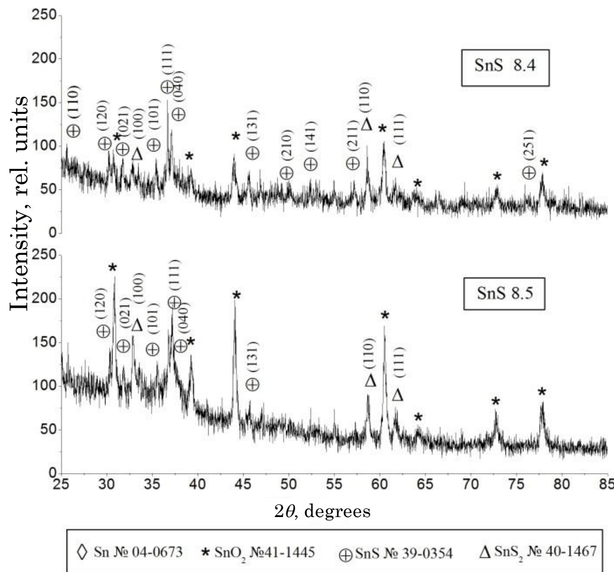

Fig. 7 – XRD patterns of tin sulfide layers obtained from electrodeposited Sn precursor by sulfurization at vertical arrangement of substrates

The optical transmission and reflection (the inset) spectra illustrated in Fig. 8 have shown that all manufactured tin sulfide layers are almost opaque and reflect little visible light, and both transmission T and reflection R decrease with increasing SnS films thicknesses. Based on the $T(\lambda)$ and $R(\lambda)$ data, calculation of the optical absorption coefficients of SnS films $\alpha(\lambda)$ gave the average values of $\alpha = (3\text{-}3.5)\cdot 10^4$ cm^{-1} in the visible and near infrared range (Fig. 9) that implies good light absorption by the manufactured tin sulfide layers – the important parameter for their application in thin-film SC. Use of the formula (1) for the determination of the type of optical interband transitions and band gap allowed to reveal (Fig. 10) that the given semiconductor material is the direct band one with the band gap which is equal to $E_g \approx 1.1\text{-}1.2$ eV that is favorable for its application as the absorbing layer of thin-film SC.

Investigation of the manufactured SnS layers by the thermal probe method has shown that all of them are electron semiconductors, i.e. they have n-type conductivity. The rectilinear behavior of the dependences on the

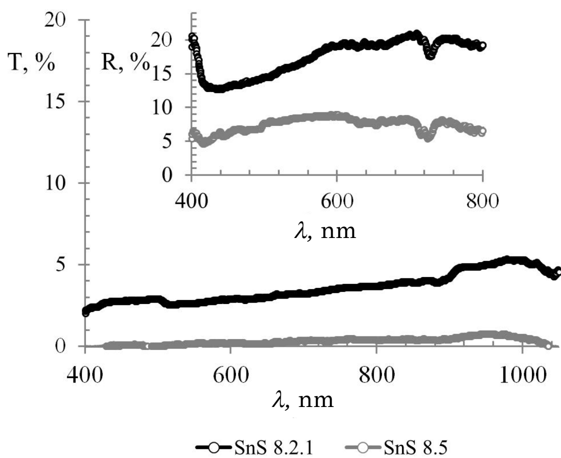

Fig. 8 – Optical transmission and reflection (the inset) spectra of tin sulfide layers: SnS 8.2.1 (d = 0.8 μm) SnS 8.5 (d = 1.8 μm)

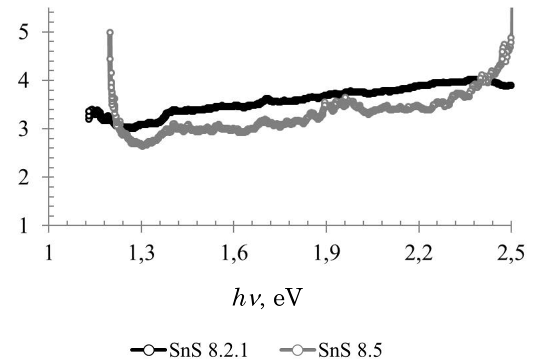

Fig. 9 – Dependence of the optical absorption coefficients α of tin sulfide layers SnS 8.2.1 and SnS 8.5 on the light quantum energy $h\nu$

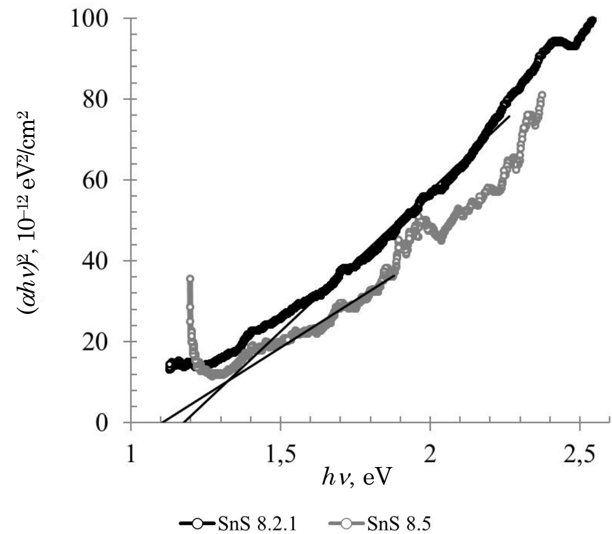

Fig. 10 – Determination of the band gap of tin sulfide layers SnS 8.2.1 and SnS 8.5 by the dependences $(\alpha(h\nu))^2$ on $h\nu$

dark CVC in the range of the current strength values of ± 100 mA (Fig. 11) has confirmed the formation of the ohmic contacts between indium and tin sulfide films, as well as between In and FTO. Calculation based on the dark CVC of the resistivity of SnS layers gave the value of $\rho_{SnS} \approx 5\text{-}9$ kOhm·cm acceptable for the use of these films as the absorbers of thin-film SC.

4. DISCUSSION

Due to the presence of two stable degrees of tin oxidation, Sn^{2+} and Sn^{4+}, formation of Sn_2S_3, Sn_3S_4 as well as tin disulfide SnS_2, which is observed by the authors of [30, 31], is quite possible in sulfurization of this metal. However, just SnS semiconductor is the most acceptable by the sum of the physical and chemical characteristics for the use as the base SC layers, since, for example, SnS_2 has wider band gap, and, therefore, cannot absorb the whole solar spectrum. Moreover, single-phase SnS film possesses the advantages from the point of view of long-term stable exploitation as part of SC. As it was found, at sulfurization of tin layers in the reactor with vertical arrangement of substrates-precursors the interaction of tin with an excess amount of sulfur vapor, wherefore tin sulfide films are found to be two-phase composed of SnS and SnS_2, is observed. However, sulfurization of tin precursors in the reactor with horizontal arrangement of

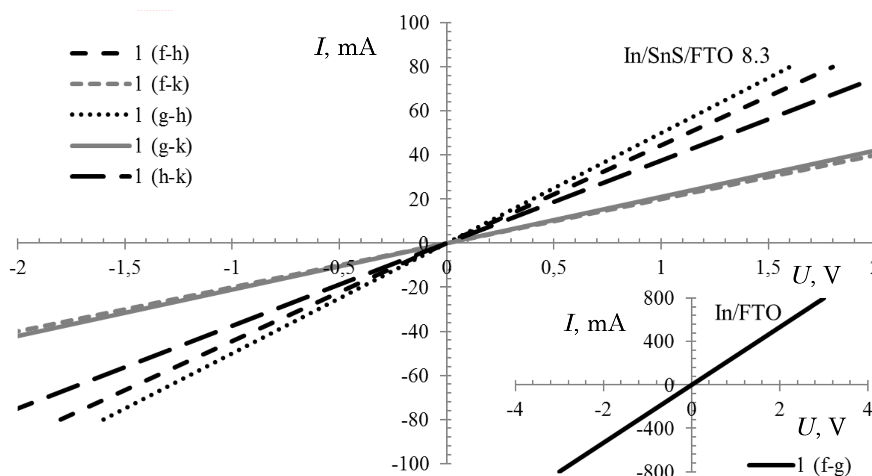

Fig. 11 – CVC of the SnS layers on the FTO substrates and CVC of the FTO substrate (the inset). Designations of the contacts correspond to Fig. 3

substrates backside to the sulfur vapor flow eliminates this disadvantage and provides the formation of single-phase β-SnS layers with more perfect crystal structure. Thus, sulfurization mode of electrodeposited tin precursors with horizontal arrangement of substrates backside to the cell with sulfur is optimum, since it provides the production of single-phase β-SnS layers. Moreover, sulfurization of several precursors simultaneously is possible for such reactor design.

Since the optical absorption coefficient α of tin sulfide layers obtained by sulfurization of electrodeposited tin precursors is more than 10^4 cm^{-1}, SnS film thicknesses less than 1 μm are enough for the total light absorption. Nevertheless, the XRD analysis has shown that tin sulfide layers of submicron thicknesses manufactured by our technique consist of very small crystallites, and therefore the acceptable thickness of sulfurized film d should be not less than 2.5 μm, and so the thickness of electrodeposited tin precursor should be more than 1.5 μm.

5. CONCLUSIONS

We have developed cost-efficient and applicable for large-scale production technique for obtaining polycrystalline layers of tin monosulfide with the orthorhombic structure (Herzenbergite, β-SnS) by sulfurization in sulfur vapor in the reactor suitable for the reuse of metal films electrodeposited from a standard tinning electrolyte. The possibility of simultaneous production of several plates with monophase SnS layers of the same structure and properties has been demonstrated. Polycrystalline SnS material we have synthesized is the electron semiconductor with the resistivity of $\rho_{\mathrm{SnS}} \approx$ 5-9 kOhm cm. The obtained SnS films are characterized by the direct optical transitions, band gap of $E_g \approx$ 1.1-1.2 eV and optical absorption coefficient of $\alpha = (3\text{-}3.5)\cdot 10^4$ cm^{-1} in the visible and near infrared range, and, consequently, by the sum of the physical and chemical characteristics they are promising for the use as the base layers of thin-film SC.

REFERENCES

1. A.M. Abdel Haleem, M. Ichimura, *J. Appl. Phys.* **107**, 034507 (2010).
2. R. Mariappan, M. Ragavendar, V. Ponnuswamy, *Optica Applicata* **XLI** No4, 989 (2011).
3. C. Cifuentes, M. Botero, E. Romero, C. Calder´on, G. Gordillo, *Brazilian J. Phys.* **36** No3B, 1046 (2006).
4. S.A. Bashkirov, V.F. Gremenok, V.A. Ivanov, *Semiconductors* **45** No6, 749 (2011).
5. M. Devika, N. Koteeswara Reddy, F. Patolsky, K.R. Gunasekhar, *J. Appl. Phys.* **104**, 124503 (2008).
6. T.H. Patel, *The Open Surface Sci. J.* **4**, 6 (2012).
7. P. Sinsermsuksakul, K. Hartman, S.B. Kim, J. Heo, L. Sun, H.H. Park, R. Chakraborty, T. Buonassisi, R.G. Gordon, *Appl. Phys. Lett.* **102**, 053901 (2013).
8. J. Park, M. Song, W.M. Jung, W.Y. Lee, J. Lee, H. Kim, I. W. Shim, *Bull. Korean Chem. Soc.* **33** No10, 3383 (2012).
9. G.H. Yue, L.S. Wang, X. Wang, Y.Z. Chen, D.L. Peng, *Nanoscale Res. Lett.* **4**, 359 (2009).
10. L.A. Burton, A. Walsh, *Appl. Phys. Lett.* **102**, 132111 (2013).
11. M. Zhao, Y. Du, X. Yang. *Appl. Mechanics Mater.* **299**, 183 (2013).
12. S. Cheng, Y. Chen, C. Huang, G. Chen, *Thin Solid Films* **500**, 96 (2006).
13. S.A. Bashkirov, V.F. Gremenok, V.A. Ivanov, V.V. Shevtsova, *Phys. Solid State* **54** No12, 2497 (2012).
14. Akkari, C. Guasch, N. Kamoun-Turki, *J. Alloy. Compd.* **490**, 180 (2010).
15. K. Khauskroft, E. Konstebl, *Sovremennyy kurs obshchey khimii* (M.: Mir: 2002).
16. N.L. Glinka, *Obshchaya khimiya* (M.: Integral-press: 2004).
17. *Laboratornyy praktikum po fizicheskoy khimii* (Ped. I.A. Kurzinoy) (Tomsk: Izd-vo Tom. gos. arkhit.-stroit. un-ta: 2008).
18. Fairbrother, X. Fontané, V. Izquierdo-Roca, M. Espíndola-Rodríguez, S. López-Marino, M. Placidi, L. Calvo-Barrio, A. Pérez-Rodríguez, E. Saucedo, *Sol. Energ. Mat. Sol. C.* **112**, 97 (2013).
19. H. Araki, Y. Kubo, A. Mikaduki, K. Jimbo, W.S. Maw, H. Katagiri, M. Yamazaki, K. Oishi, A. Takeuchi, *Sol. Energ. Mat. Sol. C.* **93**, 996 (2009).
20. S.Ya. Grilikhes, K.I. Tikhonov, *Elektroliticheskiye i khimicheskiye pokrytiya* (L.: Khimiya: 1990).
21. P.S. Mel'nikov, *Spravochnik po gal'vanopokrytiyam v mashinostroyenii* (M.: Mashinostroyeniye: 1979).
22. *Struktura i fizicheskiye svoystva tverdogo tela: Laboratornyy praktikum* (Ped. L.S. Palatnik) (Kiev: Vishcha shkola: 1983).
23. S.V. Tsybulya, *Vvedeniye v strukturnyy analiz nanokristal-*

lov (Novosibirsk: NGU: 2008).
24. M. Devika, N. Koteeswara Reddy, F. Patolsky, K.R. Gunasekhar, *J. Appl. Phys.* **104**, 124503 (2008).
25. F. Meyzda, *Elektronnyye izmeritel'nyye pribory i metody izmereniya* (M.: Mir: 1990).
26. V.A. Titov, V.V. Rybkin, V.F. Sokolov, V.Yu. Dubrovin, S.A. Smirnov, T.G. Shikova, S.R. Chernyavskiy, *Elektronnoye materialovedeniye: Laboratornyy praktikum* (Ivanovo: Ivan. gos. khim.-tekhnol. un-t: 2003).
27. V.F. Lysov, *Praktikum po fizike poluprovodnikov* (M.: Prosveshcheniye: 1976).
28. N.P. Klochko, G.S. Khrypunov, N.D. Volkova, V.R. Kopach, A.V. Momotenko, V.N. Lubov, *Semiconductors* **48** No4, 521 (2014).
29. R.M. Hazen, L.W. Finger, *Am. Mineralogist* **63**, 289 (1978).
30. Y.-T. Lin, J.-B. Shi, Y.-C. Chen,.C.-J. Chen, P.-F. Wu, *Nanoscale Res. Lett.* **4**, 694 (2009).
31. N.R. Mathews, C.C. García, I.Z. Torres, *Mater. Sci. Semiconductor Proc.* **16**, 29 (2013).